JOURNAL OF GUIDANCE, CONTROL, AND DYNAMICS
Vol. 27, No. 3, May–June 2004

Nonlinear Missile Autopilot Design with $\theta - D$ Technique

Ming Xin* and S. N. Balakrishnan†
University of Missouri–Rolla, Rolla, Missouri 65409
Donald T. Stansbery‡
Boeing Company, St. Louis, Missouri 63166
and
Ernest J. Ohlmeyer§
Naval Surface Weapon Center, Dahlgren, Virginia 22448-5000

In this paper, a new nonlinear control method is used to design a full-envelope, hybrid bank-to-turn (BTT)/skid-to-turn (STT) autopilot for an airbreathing air-to-air missile. Through this new approach, called the $\theta - D$ method, we find approximate solutions to the Hamilton–Jacobi Bellman (HJB) equation. As a result, the resulting nonlinear feedback law can be expressed in a closed form. In this paper, a $\theta - D$ outer-loop and inner-loop controller structure is used in an autopilot design. A hybrid BTT/STT autopilot command logic is used to convert the commanded accelerations from the guidance laws to reference angle commands for the autopilot. The outer-loop $\theta - D$ controller converts the angle-of-attack, sideslip, and bank-angle commands to body-rate commands for the inner loop. An inner-loop $\theta - D$ controller converts the body-rate commands to fin commands. This design is evaluated using a detailed six-degrees-of-freedom simulation. Numerical results show that the new controllers achieve excellent tracking performance and exhibit insensitivity to parameter variations over a wide flight envelope.

Nomenclature

a_y^I, a_z^I	=	acceleration along the inertial y and z axis
C_A	=	axial-force coefficient
C_l	=	roll-moment coefficient
C_{l_p}	=	roll-moment coefficient with respect to roll rate
$C_{l_{\delta p}}, C_{l_{\delta q}}, C_{l_{\delta r}}$	=	roll-moment coefficients with respect to aileron, elevator, and rudder fin, respectively
C_{l_0}	=	roll-moment coefficient with zero fin deflections
C_m	=	pitch-moment coefficient
C_{m_q}	=	pitch-moment coefficient with respect to pitch rate
$C_{m_{\delta p}}, C_{m_{\delta q}}, C_{m_{\delta r}}$	=	pitch-moment coefficients with respect to aileron, elevator, and rudder fin, respectively
C_{m_0}	=	pitch-moment coefficient with zero fin deflections
$C_{N_{\delta p}}, C_{N_{\delta q}}, C_{N_{\delta r}}$	=	normal-force coefficients with respect to aileron, elevator, and rudder fin, respectively
C_{N_0}, C_{Y_0}	=	normal- and side-force coefficients with zero fin deflections
C_n	=	yaw-moment coefficient
C_{n_r}	=	yaw-moment coefficient with respect to yaw rate
C_{n_0}	=	yaw-moment coefficient with zero fin deflections
$C_{r_{\delta p}}, C_{r_{\delta q}}, C_{r_{\delta r}}$	=	yaw-moment coefficient with respect to aileron, elevator, and rudder fin, respectively
C_Y	=	side-force coefficient
$C_{Y_{\delta p}}, C_{Y_{\delta q}}, C_{Y_{\delta r}}$	=	side-force coefficients with respect to aileron, elevator, and rudder fin, respectively
$C_Z(-C_N)$	=	normal force coefficient
d	=	missile diameter
g	=	gravity
h	=	missile flight altitude
I_x, I_y, I_z	=	moments of inertia about body frame
M	=	Mach number
m	=	missile mass
p, q, r	=	body-frame roll, pitch and yaw rate
$\bar{q}$	=	dynamic pressure
S	=	missile cross-sectional area
T	=	thrust
V	=	missile speed
α	=	angle of attack
β	=	sideslip angle
γ	=	flight-path angle
$\delta p, \delta q, \delta r$	=	aileron, elevator, and rudder fin deflections
μ	=	bank angle about the velocity vector

I. Introduction

MISSILE and aircraft autopilot designs have been mostly dominated by classical control techniques. They require a great deal of tuning, and ad hoc modifications are often unavoidable. Cloutier et al.[1] surveyed on the classical designs as well as a variety of gain-scheduled modern control designs such as linear quadratic Gaussian/loop transfer recovery (LQG/LTR) and eigenstructure assignment in the context of bank-to-turn missile autopilot designs. Gain scheduling has produced many highly reliable and effective control systems. The drawback of this method is that information about the actual nonlinear behavior is usually discarded. Williams et al.[2] proposed a gain-scheduled LQG controller to account for nonlinear kinematic coupling terms by scheduling the linear pitch/yaw channel gains as a function of both dynamic pressure and body-axis roll rate. This approach achieved good performance over a range of operating conditions although unsuitable for high-angle-of-attack maneuvering because it does not consider the aerodynamic nonlinearities. Krause and Stein[3] presented an adaptive longitudinal autopilot scheduled on the basis of an estimated pitch control derivative. Kamen et al.[4] synthesized an adaptive autopilot for a

Received 15 March 2003; revision received 19 November 2003; accepted for publication 2 December 2003.

*Postdoctoral Research Fellow, Department of Mechanical and Aerospace Engineering and Engineering Mechanics; xin@umr.edu. Member AIAA.
†Professor, Department of Mechanical and Aerospace Engineering and Engineering Mechanics; bala@umr.edu. Associate Fellow AIAA.
‡Research Scientist, Phantom Works, P.O. Box 516; Donald.t.stansbery@boeing.com. Senior Member AIAA.
§Scientist, Attn: G23, 17320 Dahlgren Road. Associate Fellow AIAA.

discrete-time linear-time-varying missile model. Tan et al.[5] applied linear-parameter-varying control theory to the design of a gain-scheduled missile autopilot.

A number of nonlinear control methods have also been proposed for the missile autopilot design. Dynamic inversion (DI) was used for the inner-loop design in the inner/outer loop control structure first proposed by Adams and Banda[6] and Adams et al.[7] In the inner loop the plant dynamics are equalized across the flight envelope using DI. μ synthesis was employed to design the outer loop to achieve performance and robustness requirements. McFarland and D'Souza[8] also combined dynamic inversion control and μ synthesis in the missile autopilot design. Because DI replaces the set of existing dynamics with a designer selected set of dynamics, Georgie and Valasek[9] attempted to quantify the particular form of desired dynamics that produce the best closed-loop performance and robustness in a DI flight controller. Schumacher and Khargonekar[10] compared gain-scheduled H_∞ control with dynamic inversion using linearized analysis and found that the latter lacked in robustness. Wise and Sedwick[11] applied nonlinear H_∞ theory to a missile with coupled aerodynamic and thrust-vectoring control. However, they showed that the nonlinear design did not significantly improve the performance of a well-designed gain-scheduled linear autopilot. There are also examples of missile autopilot designs using sliding mode control.[12–15]

Another recently emerging technique that systematically solves the nonlinear regulator problem is the state-dependent Riccati equation (SDRE) method.[16] By turning the equations of motion into a linear-like structure, this approach permits the designer to employ linear optimal control methods such as the linear-quadratic-regulator methodology and the H_∞ design technique for the synthesis of nonlinear control systems. It can be used for a broad class of nonlinear regulator problems. It has been employed to design advanced guidance algorithms in Ref. 17 and used in Ref. 18 for integrated missile guidance and control design. Wise and Sedwick[19] also reformulated their earlier nonlinear H_∞ missile autopilot design[11] using the SDRE framework, which led to a simplified feedback control form for this nonlinear control application. The SDRE method, however, needs online computation of the algebraic Riccati equation at each sample time. The $\theta - D$ method developed in this study though similar to the SDRE technique has a closed-form solution.

In this paper, the $\theta - D$ approach is formulated as a way to find an approximate solution to the Hamilton–Jacobi–Bellman (HJB) equation. By introducing an intermediate variable θ, the costate λ can be expanded as a power series in terms of θ. The HJB equation is then reduced to a set of recursive algebraic equations. By adding perturbations to the cost function and manipulating these terms appropriately, semiglobal asymptotic stability can be achieved.[20] By adjusting the parameters in the perturbation terms, we are also able to modulate the transient performance of the system.

There are two basic modes of controlling the attitude of a missile to achieve the acceleration commanded by the guidance law: skid-to-turn (STT) and bank-to-turn (BTT). In the STT mode, the roll angle can be held constant or uncontrolled. The major advantage of STT is its faster response. A BTT missile allows only positive angles of attack while maintaining small sideslip angles to prevent missile maneuvers from shading the inlet in order to increase engine efficiency and thereby maximize range. In this paper, we apply the $\theta - D$ technique to design a hybrid BTT/STT autopilot for an air-to-air missile to use their respective advantages.

It is an accepted result in flight mechanics that the flight control problem is structured in two layers. The motion of the center of gravity is addressed in the outer loop while the angular motion around the center of gravity is taken care of by the inner loop. Likewise, the control structure can also be structured into an outer-loop control, which provide the servotracking of prescribed flight angle command and the inner-loop control providing servotracking of angular rates. Tournes and Johnson[21] developed an inner-loop controller for a combat aircraft based on subspace stabilization control Theory to track the attitude rates. The outer-loop controller was designed with the linear adaptive technique to follow the flight path and ground track angles. Good results were obtained in both tracking performance and robustness. The SDRE technique is used in Ref. 22 to design the inner/outer-loop, full-envelope autopilot for bank-to-turn/skid-to-turn missiles from an optimal control point of view

This paper is organized as follows: The $\theta - D$ approximation method is formulated in Sec. II. In Sec. III, the missile dynamics are described. The $\theta - D$ inner/outer-loop autopilot design is presented in Sec. IV. In Sec. V, the BTT/STT command logic is presented. Simulation results and analysis are given in Sec. VI. Conclusions are made in Sec. VII.

II. $\theta - D$ Suboptimal Control Method

In this paper we consider optimal control of systems of the form

$$\dot{x} = \boldsymbol{f}(\boldsymbol{x}) + B(\boldsymbol{x})\boldsymbol{u} \tag{1}$$

with a cost function given by

$$J = \frac{1}{2}\int_0^\infty [x^T Q(\boldsymbol{x})\boldsymbol{x} + u^T Ru]\,\mathrm{d}t \tag{2}$$

where $\boldsymbol{x} \in R^n$, $\boldsymbol{f} \in R^n$, $B \in R^{n\times m}$, $\boldsymbol{u} \in R^m$, $Q \in R^{n\times n}$, and $R \in R^{m\times m}$. Assume that $\boldsymbol{x} \in \Omega$ and Ω is a compact set in R^n; $Q(\boldsymbol{x})$ is semipositive definite, and R is a positive definite constant matrix. It is assumed that $\boldsymbol{f}(0) = 0$.

To ensure that the control problem is well posed, we assume that a solution to the optimal control problem (1), (2) exists. We also assume that $\boldsymbol{f}(\boldsymbol{x})$ is of class C^1 in $\boldsymbol{x}$ on a compact set Ω and zero state observable through Q.

The optimal solution of the infinite-horizon nonlinear regulator problem can be obtained by solving the HJB partial differential equation[23]

$$\frac{\partial V^T}{\partial \boldsymbol{x}}\boldsymbol{f}(\boldsymbol{x}) - \frac{1}{2}\frac{\partial V^T}{\partial \boldsymbol{x}}B(\boldsymbol{x})R^{-1}B^T(\boldsymbol{x})\frac{\partial V}{\partial \boldsymbol{x}} + \frac{1}{2}x^T Q(\boldsymbol{x})\boldsymbol{x} = 0 \tag{3}$$

where $V(\boldsymbol{x})$ is the optimal cost, that is,

$$V(\boldsymbol{x}) = \min_u \frac{1}{2}\int_0^\infty [x^T Q(\boldsymbol{x})\boldsymbol{x} + u^T Ru]\,\mathrm{d}t \tag{4}$$

We assume that $V(\boldsymbol{x})$ is continuously differentiable and $V(\boldsymbol{x}) > 0$ with $V(0) = 0$.

Optimal control is given by

$$\boldsymbol{u} = -R^{-1}B^T(\boldsymbol{x})\frac{\partial V}{\partial \boldsymbol{x}} \tag{5}$$

The HJB equation is extremely difficult to solve in general, rendering optimal control techniques of limited use for nonlinear systems.

Now consider perturbations added to the cost function:

$$J = \frac{1}{2}\int_0^\infty \left\{x^T\left[Q(\boldsymbol{x}) + \sum_{i=1}^\infty D_i\theta^i\right]\boldsymbol{x} + u^T Ru\right\}\mathrm{d}t \tag{6}$$

where θ and D_i are chosen such that

$$Q(\boldsymbol{x}) + \sum_{i=1}^\infty D_i\theta^i$$

is semipositive definite.

Write the original state equation as

$$\dot{x} = \boldsymbol{f}(\boldsymbol{x}) + B(\boldsymbol{x})\boldsymbol{u} = \{A_0 + \theta[A(\boldsymbol{x})/\theta]\}\boldsymbol{x} + \{g_0 + \theta[g(\boldsymbol{x})/\theta]\}\boldsymbol{u} \tag{7}$$

where A_0 and g_0 are constant matries such that (A_0, g_0) is a stabilizable pair and $\{[A_0 + A(\boldsymbol{x})], [g_0 + g(\boldsymbol{x})]\}$ is pointwise controllable. Also write the perturbed cost function as

$$J = \frac{1}{2}\int_0^\infty \left\{x^T\left[Q_0 + \theta\frac{Q_x(\boldsymbol{x})}{\theta} + \sum_{i=1}^\infty D_i\theta^i\right]\boldsymbol{x} + u^T Ru\right\}\mathrm{d}t \tag{8}$$

such that $Q(\boldsymbol{x}) = Q_0 + Q_x(\boldsymbol{x})$ and Q_0 is a constant matrix. Define

$$\lambda = \frac{\partial V}{\partial \boldsymbol{x}} \tag{9}$$

By using Eqs. (8) and (9) in HJB equation (3), we have the perturbed HJB equation

$$\lambda^T \boldsymbol{f}(\boldsymbol{x}) - \frac{1}{2}\lambda^T B(\boldsymbol{x}) R^{-1} B^T(\boldsymbol{x})\lambda + \frac{1}{2}x^T\left[Q_0 + \theta\frac{Q_x(\boldsymbol{x})}{\theta} + \sum_{i=1}^{\infty} D_i\theta^i\right]\boldsymbol{x} = 0 \tag{10}$$

Assume a power series expansion of λ in terms of θ:

$$\lambda = \frac{\partial V}{\partial \boldsymbol{x}} = \sum_{i=0}^{\infty} T_i\theta^i \boldsymbol{x} \tag{11}$$

where T_i are assumed to be symmetric and to be determined.

Substitute Eq. (11) into the HJB equation (10) and equate the coefficients of powers of θ to zero to get the following equations:

$$T_0A_0 + A_0^T T_0 - T_0 g_0 R^{-1} g_0^T T_0 + Q_0 = 0 \tag{12}$$

$$\begin{aligned} T_1\left(A_0 - g_0R^{-1}g_0^T T_0\right) + \left(A_0^T - T_0 g_0 R^{-1} g_0^T\right)T_1 &= -\frac{T_0A(\boldsymbol{x})}{\theta} - \frac{A^T(\boldsymbol{x})T_0}{\theta} + T_0 g_0 R^{-1}\frac{g^T}{\theta}T_0 \\ &\quad + T_0\frac{g}{\theta}R^{-1}g_0^T T_0 - D_1 - \frac{Q_x(\boldsymbol{x})}{\theta} \end{aligned} \tag{13}$$

$$\begin{aligned} T_2\left(A_0 - g_0R^{-1}g_0^T T_0\right) + \left(A_0^T - T_0 g_0 R^{-1} g_0^T\right)T_2 &= -\frac{T_1A(\boldsymbol{x})}{\theta} - \frac{A^T(\boldsymbol{x})T_1}{\theta} + T_0 g_0 R^{-1}\frac{g^T}{\theta}T_1 \\ &\quad + T_0\frac{g}{\theta}R^{-1}g_0^T T_1 + T_0\frac{g}{\theta}R^{-1}\frac{g^T}{\theta}T_0 + T_1 g_0 R^{-1} g_0^T T_1 \\ &\quad + T_1 g_0 R^{-1}\frac{g^T}{\theta}T_0 + T_1\frac{g}{\theta}R^{-1}g_0^T T_0 - D_2 \\ &\vdots \end{aligned} \tag{14}$$

$$\begin{aligned} T_n\left(A_0 - g_0R^{-1}g_0^T T_0\right) + \left(A_0^T - T_0 g_0 R^{-1} g_0^T\right)T_n &= -\frac{T_{n-1}A(\boldsymbol{x})}{\theta} - \frac{A^T(\boldsymbol{x})T_{n-1}}{\theta} - D_n \\ &\quad + \sum_{j=0}^{n-1} T_j\left(g_0R^{-1}\frac{g^T}{\theta} + \frac{g}{\theta}R^{-1}g_0^T\right)T_{n-1-j} \\ &\quad + \sum_{j=0}^{n-2} T_j\frac{g}{\theta}R^{-1}\frac{g^T}{\theta}T_{n-2-j} + \sum_{j=1}^{n-1} T_j g_0 R^{-1} g_0^T T_{n-j} \end{aligned} \tag{15}$$

Because the right-hand side of equations (12–15) involves $\boldsymbol{x}$ and θ, T_i would be a function of $\boldsymbol{x}$ and θ. Thus we denote it as $T_i(\boldsymbol{x}, \theta)$. The expression for control can be obtained in terms of the power series:

$$\boldsymbol{u} = -R^{-1}B^T(\boldsymbol{x})\frac{\partial V}{\partial \boldsymbol{x}} = -R^{-1}B^T(\boldsymbol{x})\sum_{i=0}^{\infty} T_i(\boldsymbol{x},\theta)\theta^i\boldsymbol{x} \tag{16}$$

It is easy to see that Eq. (12) is an algebraic Riccati equation. The rest of equations are Lyapunov equations that are linear in terms of $T_i (i = 1 \cdots n)$.

We construct the following expression for D_i, $i = 1, \cdots n$:

$$D_1 = k_1 e^{-l_1 t}\left[-\frac{T_0A(\boldsymbol{x})}{\theta} - \frac{A^T(\boldsymbol{x})T_0}{\theta} + T_0 g_0 R^{-1}\frac{g^T}{\theta}T_0 + T_0\frac{g}{\theta}R^{-1}g_0^T T_0 - \frac{Q_x(\boldsymbol{x})}{\theta}\right] \tag{17}$$

$$\begin{aligned} D_2 = k_2 e^{-l_2 t}\Bigg[&-\frac{T_1A(\boldsymbol{x})}{\theta} - \frac{A^T(\boldsymbol{x})T_1}{\theta} + T_0 g_0 R^{-1}\frac{g^T}{\theta}T_1 \\ &+ T_0\frac{g}{\theta}R^{-1}g_0^T T_1 + T_0\frac{g}{\theta}R^{-1}\frac{g^T}{\theta}T_0 + T_1 g_0 R^{-1}\frac{g^T}{\theta}T_0 \\ &+ T_1\frac{g}{\theta}R^{-1}g_0^T T_0 + T_1 g_0 R^{-1} g_0^T T_1\Bigg] \end{aligned} \tag{18}$$

$$\vdots$$

$$\begin{aligned} D_n = k_n e^{-l_n t}\Bigg[&-\frac{T_{n-1}A(\boldsymbol{x})}{\theta} - \frac{A^T(\boldsymbol{x})T_{n-1}}{\theta} \\ &+ \sum_{j=0}^{n-1} T_j\left(g_0R^{-1}\frac{g^T}{\theta} + \frac{g}{\theta}R^{-1}g_0^T\right)T_{n-1-j} \\ &+ \sum_{j=0}^{n-2} T_j\frac{g}{\theta}R^{-1}\frac{g^T}{\theta}T_{n-2-j} + \sum_{j=1}^{n-1} T_j g_0 R^{-1} g_0^T T_{n-j}\Bigg] \end{aligned} \tag{19}$$

where k_i and $l_i > 0$, $i = 1, \cdots n$ are adjustable design parameters.

The idea in constructing D_i in this manner is based on the observation that large initial states can give rise to large initial control as a result of the state-dependent term $A(\boldsymbol{x})$ on the right-hand side of Eqs. (13–15). It happens when there are some terms in $A(\boldsymbol{x})$ that could grow to a high magnitude as $\boldsymbol{x}$ is large. To see this, for example, when $A(\boldsymbol{x})$ includes a cubic term, its magnitude could be large if $\boldsymbol{x}$ is large. This large value will be reflected into the solution for T_i, that is, the left-hand side of Eqs. (13–15). Because T_i will be used in the next equation to solve for T_{i+1}, this large value will be propagated and amplified and consequently cause higher control or even instability. So if we choose D_i such that

$$\begin{aligned} -\frac{T_{i-1}A(\boldsymbol{x})}{\theta} - \frac{A^T(\boldsymbol{x})T_{i-1}}{\theta} + \sum_{j=0}^{i-1} T_j\left(g_0R^{-1}\frac{g^T}{\theta} + \frac{g}{\theta}R^{-1}g_0^T\right)T_{i-1-j} &\\ + \sum_{j=0}^{i-2} T_j\frac{g}{\theta}R^{-1}\frac{g^T}{\theta}T_{i-2-j} + \sum_{j=0}^{i-1} T_j g_0 R^{-1} g_0^T T_{i-j} - D_i &\\ = \varepsilon_i(t)\Bigg[-\frac{T_{i-1}A(\boldsymbol{x})}{\theta} - \frac{A^T(\boldsymbol{x})T_{i-1}}{\theta} &\\ + \sum_{j=0}^{i-1} T_j\left(g_0R^{-1}\frac{g^T}{\theta} + \frac{g}{\theta}R^{-1}g_0^T\right)T_{i-1-j} &\\ + \sum_{j=0}^{i-2} T_j\frac{g}{\theta}R^{-1}\frac{g^T}{\theta}T_{i-2-j} + \sum_{j=0}^{i-1} T_j g_0 R^{-1} g_0^T T_{i-j}\Bigg] & \end{aligned} \tag{20}$$

where

$$\varepsilon_i(t) = 1 - k_i e^{-l_i t} \tag{21}$$

is a small number, ε_i can be used to suppress this large value from propagating in Eqs. (13–15). $\varepsilon_i(t)$ is chosen to satisfy some conditions required in the proof of convergence and stability of the preceding algorithm.[20] On the other hand, the exponential term $e^{-l_i t}$ with $l_i > 0$ is used to let the perturbation terms in the cost function and HJB equation diminish as time evolves.

Remark 2.1: Solving Eqs. (12–15) is carried out offline successively from top to bottom, that is, T_n can be solved from T_{n-1}.

Equation (12) is a standard algebraic Riccati equation. Once A_0, g_0, Q_0, and R are determined, T_0 can be solved to be a constant matrix. The rest of Eqs. (13–15) are linear equations in terms of $T_2, \ldots, T_n$ with constant coefficients $(A_0 - g_0 R^{-1} g_0^T T_0)$ and $(A_0^T - T_0 g_0 R^{-1} g_0^T)$ once we obtain the solution for T_0 from Eq. (12). With some linear algebra, Eqs. (13–15) can be rearranged in the form of $\hat{A}_0 T_i = Q_i(\boldsymbol{x}, \theta, t)$. As a result, T_i can be written in a closed form, $T_i = \hat{A}_0^{-1} Q_i(\boldsymbol{x}, \theta, t)$, where $\hat{A}_0$ is a constant matrix. So we can get closed-form solutions to $T_2, \ldots, T_n$ with just one matrix inverse operation. The expression of $Q_i(\boldsymbol{x}, \theta, t)$ on the right-hand side of the equations is already known and only needs simple matrix multiplications and additions.

Remark 2.2: The construction of D_i in Eqs. (17–20) serves three functions. The first is to suppress the large control if it happens. The second is to provide an appropriate ε_i to guarantee the convergence of power series expansion

$$\sum_{i=0}^{\infty} T_i(\boldsymbol{x}, \theta)\theta^i$$

and stability of the closed-loop system.[20] The third function is to allow flexibility to modulate the system performance by tuning the parameters of k_i and l_i in the D_i. This will be shown in the autopilot design.

Remark 2.3: θ is just an intermediate variable and its value can be kept as unity.

III. Missile Dynamics

Equations of motion of a generic air-to-air missile dynamics are given next[22] in terms of missile's speed V, angle of attack α, sideslip β, bank angle μ, roll rate p, pitch rate q, and yaw rate r:

$$\begin{aligned}\dot{V} =& -\frac{\bar{q}S}{m}C_A \cos\alpha\cos\beta + \frac{\bar{q}S}{m}C_{Y_0}\sin\beta - \frac{\bar{q}S}{m}C_{N_0}\sin\alpha\cos\beta \\ & - g\sin\gamma + \frac{\cos\alpha\cos\beta}{m}T + \frac{\bar{q}S}{m}\Big[\Big(C_{Y_{\delta p}}\sin\beta \\ & - C_{N_{\delta p}}\sin\alpha\cos\beta\Big)\delta p - \Big(C_{Y_{\delta q}}\sin\beta - C_{N_{\delta q}}\sin\alpha\cos\beta\Big)\delta q \\ & - \Big(C_{Y_{\delta r}}\sin\beta - C_{N_{\delta r}}\sin\alpha\cos\beta\Big)\delta r\Big] \qquad (22)\end{aligned}$$

$$\begin{aligned}\dot{\alpha} =& \, q - \tan\beta\cos\alpha p - \tan\beta\sin\alpha r + \frac{g}{V\cos\beta}\cos\gamma\cos\mu \\ & - \frac{\bar{q}S}{mV\cos\beta}C_{N_0}\cos\alpha + \frac{\bar{q}S}{mV\cos\beta}C_A\sin\alpha - \frac{\sin\alpha}{mV\cos\beta}T \\ & - \frac{\bar{q}S\cos\alpha}{mV\cos\beta}\Big(C_{N_{\delta p}}\delta p - C_{N_{\delta q}}\delta q - C_{N_{\delta r}}\delta r\Big) \qquad (23)\end{aligned}$$

$$\begin{aligned}\dot{\beta} =& \sin\alpha p - \cos\alpha r + \frac{g}{V}\cos\gamma\sin\mu + \frac{\bar{q}S}{mV}C_{N_0}\sin\alpha\sin\beta \\ & + \frac{\bar{q}S}{mV}C_A\cos\alpha\sin\beta + \frac{\bar{q}S}{mV}C_{Y_0}\cos\beta - \frac{\cos\alpha\sin\beta}{mV}T \\ & + \frac{\bar{q}S}{mV}\Big[\Big(C_{Y_{\delta p}}\cos\beta + C_{N_{\delta p}}\sin\alpha\sin\beta\Big)\delta p \\ & - \Big(C_{Y_{\delta q}}\cos\beta - C_{N_{\delta q}}\sin\alpha\sin\beta\Big)\delta q \\ & - \Big(C_{Y_{\delta r}}\cos\beta - C_{N_{\delta r}}\sin\alpha\sin\beta\Big)\delta r\Big] \qquad (24)\end{aligned}$$

$$\begin{aligned}\dot{\mu} =& \, p\frac{\cos\alpha}{\cos\beta} + r\frac{\sin\alpha}{\cos\beta} + \frac{T}{mV}[\sin\alpha\sin\mu\tan\gamma \\ & - \cos\alpha\sin\beta\cos\mu\tan\gamma + \sin\alpha\tan\beta] \\ & + C_{N_0}\cos\alpha(\sin\mu\tan\gamma + \tan\beta) \\ & + \frac{\bar{q}S}{mV}\big[-C_A\sin\alpha(\sin\mu\tan\gamma + \tan\beta) \\ & + C_A\cos\alpha\cos\mu\sin\beta\tan\gamma + C_{N_0}\sin\alpha\cos\mu\sin\beta\tan\gamma \\ & + C_{N_0}\cos\alpha(\sin\mu\tan\gamma + \tan\beta) \\ & + C_{Y_0}\cos\mu\cos\beta\tan\gamma\big] - \frac{g}{V}\cos\gamma\cos\mu\tan\beta \\ & + \frac{\bar{q}S}{mV}\Big(C_{N_{\delta p}}\delta p - C_{N_{\delta q}}\delta q - C_{N_{\delta r}}\delta r\Big) \\ & \times[\cos\alpha(\sin\mu\tan\gamma + \tan\beta) + \sin\alpha\cos\mu\sin\beta\tan\gamma] \\ & + \frac{\bar{q}S}{mV}\Big(C_{Y_{\delta p}}\delta p - C_{Y_{\delta q}}\delta q - C_{Y_{\delta r}}\delta r\Big)\cos\mu\cos\beta\tan\gamma \qquad (25)\end{aligned}$$

$$\begin{aligned}\dot{p} =& \frac{I_y - I_z}{I_x}qr + \frac{\bar{q}Sd^2}{2I_xV}\Big(C_{l_p}\cos\alpha p - C_{n_r}\sin\alpha r\Big) \\ & + \frac{\bar{q}Sd}{I_x}\Big(C_{l_0}\cos\alpha - C_{n_0}\sin\alpha\Big) + \frac{\bar{q}Sd}{I_x}\Big[\Big(C_{l_{\delta p}}\cos\alpha \\ & - C_{n_{\delta p}}\sin\alpha\Big)\delta p - \Big(C_{l_{\delta q}}\cos\alpha - C_{n_{\delta q}}\sin\alpha\Big)\delta q \\ & - \Big(C_{l_{\delta r}}\cos\alpha - C_{n_{\delta r}}\sin\alpha\Big)\delta r\Big] \qquad (26)\end{aligned}$$

$$\begin{aligned}\dot{q} =& \frac{I_z - I_x}{I_y}rp + \frac{\bar{q}Sd^2}{2I_yV}C_{m_q}q \\ & + \frac{\bar{q}Sd}{I_y}\Big(C_{m_0} + C_{m_{\delta p}}\delta p - C_{m_{\delta q}}\delta q - C_{m_{\delta r}}\delta r\Big) \qquad (27)\end{aligned}$$

$$\begin{aligned}\dot{r} =& \frac{I_x - I_y}{I_z}pq + \frac{\bar{q}Sd^2}{2I_zV}\Big(C_{l_p}\sin\alpha p + C_{n_r}\cos\alpha r\Big) \\ & + \frac{\bar{q}Sd}{I_z}\Big(C_{l_0}\sin\alpha + C_{n_0}\cos\alpha\Big) + \frac{\bar{q}Sd}{I_z}\Big[\Big(C_{l_{\delta p}}\sin\alpha \\ & + C_{n_{\delta p}}\cos\alpha\Big)\delta p - \Big(C_{l_{\delta q}}\sin\alpha + C_{n_{\delta q}}\cos\alpha\Big)\delta q \\ & - \Big(C_{l_{\delta r}}\sin\alpha + C_{n_{\delta r}}\cos\alpha\Big)\delta r\Big] \qquad (28)\end{aligned}$$

IV. $\theta - D$ Autopilot Design

A. Outer-Loop and Inner-Loop Tracking Structure

The autopilot design is performed in a two-loop structure shown in Fig. 1. Acceleration commands from the missile guidance law are converted to α_c, β_c, and μ_c, which are angle-of-attack, sideslip, and bank-angle commands, respectively, by using the BTT/STT logic, which will be presented in Sec. V. The outer loop converts α_c, β_c, and μ_c to roll-rate, pitch-rate, and yaw-rate commands p_c, q_c, and r_c, respectively, for the inner loop. The inner loop then converts p_c, q_c, and r_c to fin commands δ_{p_c}, δ_{q_c}, and δ_{r_c} for the actuators.

To design the autopilot to perform command following, the $\theta - D$ outer-loop controller is implemented as an integral servomechanism.[24] This is accomplished as follows: First, the state $\boldsymbol{x}$ is decomposed as

$$\boldsymbol{x} = [\boldsymbol{x}_T \quad \boldsymbol{x}_N]^T \qquad (29)$$

where $\boldsymbol{x}_T$ consists of the tracked states, which should track a reference command $\tilde{\boldsymbol{r}}_c$ and $\boldsymbol{x}_N$ consists of the nontracked states. The state vector $\boldsymbol{x}$ is then augmented with $\boldsymbol{x}_I$, the integral states of $\boldsymbol{x}_T$:

$$\tilde{\boldsymbol{x}} = [\boldsymbol{x}_I \quad \boldsymbol{x}_T \quad \boldsymbol{x}_N]^T \qquad (30)$$

The augmented system is given by

$$\dot{\tilde{x}} = \tilde{f}(\tilde{\boldsymbol{x}}) + \tilde{B}(\tilde{\boldsymbol{x}})\boldsymbol{u} \qquad (31)$$

where

$$\tilde{B}(\tilde{\boldsymbol{x}}) = \begin{bmatrix} 0 \\ B(\boldsymbol{x}) \end{bmatrix} \qquad (32)$$

So the problem addressed here is to find an optimal controller to minimize the cost functional

$$J = \frac{1}{2}\int_0^{\infty} [\tilde{\boldsymbol{x}}^T \tilde{Q}(\tilde{\boldsymbol{x}})\tilde{\boldsymbol{x}} + u^T \tilde{R} u]\,\mathrm{d}t \qquad (33)$$

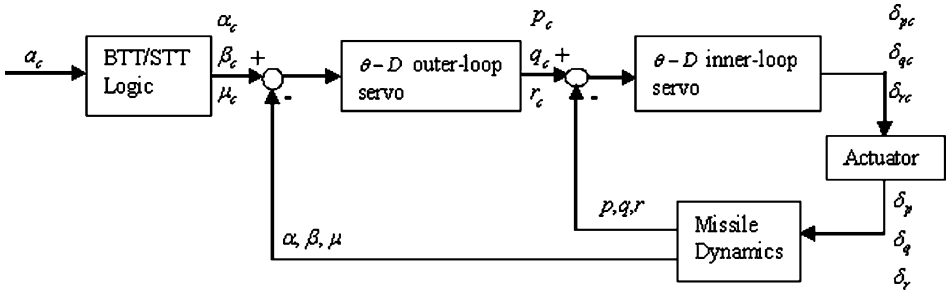

Fig. 1 $\theta - D$ outer-loop and inner-loop autopilot structure.

The $\theta - D$ integral controller is given by

$$\boldsymbol{u} = -\tilde{R}(\tilde{\boldsymbol{x}})^{-1}\tilde{B}(\tilde{\boldsymbol{x}})^T \sum_{n=0}^{\infty} T_n(\tilde{\boldsymbol{x}}, \theta)\theta^n \begin{bmatrix} \boldsymbol{x}_I - \int \tilde{\boldsymbol{r}}_c \, \mathrm{d}t \\ \boldsymbol{x}_T - \tilde{\boldsymbol{r}}_c \\ \boldsymbol{x}_N \end{bmatrix} \tag{34}$$

where $\tilde{\boldsymbol{r}}_c$ is the command that it is desired to track. In the $\theta - D$ controller design, use of the first three terms in

$$\sum_{n=0}^{\infty} T_n(\tilde{\boldsymbol{x}}, \theta)\theta^n$$

has been found to be accurate enough for this problem (as well as some others that have been solved).

In the $\theta - D$ formulation, we choose the factorization of nonlinear equation (7) in this way:

$$\dot{\tilde{\boldsymbol{x}}} = (\tilde{A}(\tilde{\boldsymbol{x}}_0) + \theta\{[\tilde{A}(\tilde{\boldsymbol{x}}) - \tilde{A}(\tilde{\boldsymbol{x}}_0)]/\theta\})\tilde{\boldsymbol{x}} + (\tilde{B}(\tilde{\boldsymbol{x}}_0) + \theta\{[\tilde{B}(\tilde{\boldsymbol{x}}) - \tilde{B}(\tilde{\boldsymbol{x}}_0)]/\theta\})\boldsymbol{u} \tag{35}$$

The advantage of choosing this factorization is that in the $\theta - D$ formulation T_0 is solved from A_0 and g_0 in Eq. (7) and Eq. (12). If we select $A_0 = \tilde{A}(\tilde{\boldsymbol{x}}_0)$ and $g_0 = \tilde{B}(\tilde{\boldsymbol{x}}_0)$, we would have a good starting point for T_0 because $\tilde{A}(\tilde{\boldsymbol{x}}_0)$ and $\tilde{B}(\tilde{\boldsymbol{x}}_0)$ keep much more system information than an arbitrary choice of A_0 and g_0.

B. $\theta - D$ Outer-Loop Design

For the outer loop, the state space is chosen to be

$$\tilde{\boldsymbol{x}} = [V \quad \alpha_I \quad \alpha \quad \beta_I \quad \beta \quad \mu_I \quad \mu]^T \tag{36}$$

with control vector $\boldsymbol{u}$ given by

$$\boldsymbol{u} = [p, q, r]^T \tag{37}$$

The tracking command is

$$\tilde{\boldsymbol{r}}_c = [\alpha_c \quad \beta_c \quad \mu_c]^T \tag{38}$$

This command is obtained from the guidance law by using the BTT/STT logic, which will be presented in Sec. V.

The outer-loop state-dependent coefficient factorization $\tilde{A}_{\mathrm{OL}}(\tilde{\boldsymbol{x}})$ is chosen as

$$\tilde{A}_{\mathrm{OL}}(\tilde{\boldsymbol{x}}) = \begin{bmatrix} a_{11} & 0 & a_{13} & 0 & a_{15} & 0 & 0 \\ 0 & 0 & 1 & 0 & 0 & 0 & 0 \\ a_{31} & 0 & a_{33} & 0 & 0 & 0 & 0 \\ 0 & 0 & 0 & 0 & 1 & 0 & 0 \\ a_{51} & 0 & a_{53} & 0 & a_{55} & 0 & a_{57} \\ 0 & 0 & 0 & 0 & 0 & 0 & 1 \\ a_{71} & 0 & a_{73} & 0 & a_{75} & 0 & a_{77} \end{bmatrix} \tag{39}$$

where

$$\begin{aligned} a_{11} = {} & -\frac{\bar{q}S}{mV}C_A \cos\alpha\cos\beta - \frac{g}{V}\sin\gamma + \frac{T}{mV}\cos\alpha\cos\beta \\ & + \frac{\bar{q}S}{mV}\left(C_{Y_{\delta p}}\sin\beta - C_{N_{\delta p}}\sin\alpha\cos\beta\right)\delta p \\ & - \frac{\bar{q}S}{mV}(C_{Y_{\delta q}}\sin\beta - C_{N_{\delta q}}\sin\alpha\cos\beta)\delta q \\ & - \frac{\bar{q}S}{mV}\left(C_{Y_{\delta r}}\sin\beta - C_{N_{\delta r}}\sin\alpha\cos\beta\right)\delta r \end{aligned} \tag{40}$$

$$a_{13} = -\frac{\bar{q}S}{m}C_{N_0}\frac{\sin\alpha}{\alpha}\cos\beta \tag{41}$$

$$a_{15} = \frac{\bar{q}S}{m}C_{Y_0}\frac{\sin\beta}{\beta} \tag{42}$$

$$\begin{aligned} a_{31} = {} & \frac{g}{V^2\cos\beta}\cos\gamma\cos\mu - \frac{\bar{q}S}{mV^2\cos\beta}\cos\alpha C_{N_0} \\ & - \frac{\bar{q}S}{mV^2\cos\beta}\cos\alpha\left(C_{N_{\delta p}}\delta p - C_{N_{\delta q}}\delta q - C_{N_{\delta r}}\delta r\right) \end{aligned} \tag{43}$$

$$a_{33} = -\frac{T}{mV\cos\beta}\frac{\sin\alpha}{\alpha} + \frac{\bar{q}S}{mV\cos\beta}C_A\frac{\sin\alpha}{\alpha} \tag{44}$$

$$\begin{aligned} a_{51} = {} & \frac{\bar{q}S}{mV^2}C_{Y_0}\cos\beta + \left(C_{Y_{\delta p}}\cos\beta + C_{N_{\delta p}}\sin\alpha\sin\beta\right)\delta p \\ & - \left(C_{Y_{\delta q}}\cos\beta + C_{N_{\delta q}}\sin\alpha\sin\beta\right)\delta q \\ & - \left(C_{Y_{\delta r}}\cos\beta + C_{N_{\delta r}}\sin\alpha\sin\beta\right)\delta r \end{aligned} \tag{45}$$

$$a_{53} = \frac{1}{2}\frac{\bar{q}S}{mV}C_{N_0}\frac{\sin\alpha}{\alpha}\sin\beta \tag{46}$$

$$a_{55} = \frac{1}{2}\frac{\bar{q}S}{mV}C_{N_0}\sin\alpha\frac{\sin\beta}{\beta} + \left(\frac{\bar{q}S}{mV}C_A - \frac{T}{mV}\right)\cos\alpha\frac{\sin\beta}{\beta} \tag{47}$$

$$a_{57} = \frac{g}{V}\cos\gamma\frac{\sin\mu}{\mu} \tag{48}$$

$$a_{71} = \frac{\bar{q}S}{mV^2}\left(C_{Y_0} + C_{Y_{\delta p}}\delta p - C_{Y_{\delta q}}\delta q - C_{Y_{\delta r}}\delta r\right)\cos\mu\cos\beta\tan\gamma \tag{49}$$

$$\begin{aligned} a_{73} = {} & \frac{1}{2}\frac{T}{mV}\frac{\sin\alpha}{\alpha}\sin\mu\tan\gamma + \frac{1}{2}\frac{T}{mV}\frac{\sin\alpha}{\alpha}\tan\beta \\ & - \frac{1}{2}\frac{\bar{q}S}{mV}C_A\frac{\sin\alpha}{\alpha}\sin\mu\tan\gamma - \frac{1}{2}\frac{\bar{q}S}{mV}C_A\frac{\sin\alpha}{\alpha}\tan\beta \\ & + \frac{1}{2}\frac{\bar{q}S}{mV}\left(C_{N_0} + C_{N_{\delta p}}\delta p - C_{N_{\delta q}}\delta q - C_{N_{\delta r}}\delta r\right)\frac{\sin\alpha}{\alpha} \\ & \times \cos\mu\sin\beta\tan\gamma \end{aligned} \tag{50}$$

$$a_{75} = -\frac{T}{mV}\cos\alpha\frac{\sin\beta}{\beta}\cos\mu\tan\gamma + \frac{1}{2}\frac{T}{mV}\frac{1}{\cos\beta}\sin\alpha\frac{\sin\beta}{\beta} - \frac{1}{2}\frac{\bar{q}S}{mV\cos\beta}C_A\sin\alpha\frac{\sin\beta}{\beta} + \frac{\bar{q}S}{mV\cos\beta}\left(C_{N_0} + C_{N_{\delta p}}\delta p - C_{N_{\delta q}}\delta q - C_{N_{\delta r}}\delta r\right) \times \cos\alpha\frac{\sin\beta}{\beta} + \frac{\bar{q}S}{mV}C_A\cos\alpha\cos\mu\frac{\sin\beta}{\beta}\tan\gamma + \frac{1}{2}\frac{\bar{q}S}{mV}\left(C_{N_0} + C_{N_{\delta p}}\delta p - C_{N_{\delta q}}\delta q - C_{N_{\delta r}}\delta r\right)\sin\alpha\cos\mu\frac{\sin\beta}{\beta} \times \tan\gamma - \frac{g}{V\cos\beta}\cos\gamma\cos\mu\frac{\sin\beta}{\beta} \tag{51}$$

$$a_{77} = \frac{1}{2}\frac{T}{mV}\sin\alpha\frac{\sin\mu}{\mu}\tan\gamma - \frac{1}{2}\frac{\bar{q}S}{mV}C_A\sin\alpha\frac{\sin\mu}{\mu}\tan\gamma + \frac{\bar{q}S}{mV}\left(C_{N_0} + C_{N_{\delta p}}\delta p - C_{N_{\delta q}}\delta q - C_{N_{\delta r}}\delta r\right)\cos\alpha\frac{\sin\mu}{\mu}\tan\gamma \tag{52}$$

Remark 4.1: There are numerous ways of factorizing $\boldsymbol{f}(\boldsymbol{x})$ as $A(\boldsymbol{x})\boldsymbol{x}$. The principle of choosing $A(\boldsymbol{x})$ peculiar to this missile problem is to find the terms with sinusoid function such as $\sin\alpha$, $\sin\beta$, or $\sin\mu$ and write these terms as $\sin(*)/*$ in which * represents α, β, or μ. In this way we can pull out the state variables from $\boldsymbol{f}(\boldsymbol{x})$ and guarantee $\sin(*)/*$ is regular when * goes to zero.

The $\tilde{B}_{\mathrm{OL}}(\tilde{\boldsymbol{x}})$ becomes

$$\tilde{B}_{\mathrm{OL}}(\tilde{\boldsymbol{x}}) = \begin{bmatrix} 0 & 0 & 0 \\ 0 & 0 & 0 \\ -\tan\beta\cos\alpha & 1 & -\tan\beta\sin\alpha \\ 0 & 0 & 0 \\ \sin\alpha & 0 & -\cos\alpha \\ 0 & 0 & 0 \\ \dfrac{\cos\alpha}{\cos\beta} & 0 & \dfrac{\sin\alpha}{\cos\beta} \end{bmatrix} \tag{53}$$

Because p, q, and r would be the control in the outer loop, the current values of the fin deflections δp, δq, and δr are used in this loop during the simulation, which is based on Eqs. (22–25).

C. $\theta - D$ Inner-Loop Design

The objective in the inner-loop controller is to follow the commands roll rate p_c, pitch rate q_c, and yaw rate r_c, respectively, which are produced in the outer-loop controller. In the inner-loop design, we would not adopt the integral servo because our major aim is to follow the angular commands α, β, and μ, respectively, which is realized in the outer-loop controller. Tracking of the body-rate commands p, q, and r in the inner loop is used to improve the transient response of the missile.

Consider Eqs. (26–28). We notice that there are state-independent terms $\bar{q}Sd(C_{l_0}\cos\alpha - C_{n_0}\sin\alpha)/I_x$, $\bar{q}SdC_{m_0}/I_y$, and $\bar{q}Sd(C_{l_0}\sin\alpha + C_{n_0}\cos\alpha)/I_z$ that will not go to zero when the inner-loop states approach zero. To see this, note that V and α, the state variables in the outer loop, are considered as constants in the inner loop. As a result, $\bar{q}$ is not a function of any state variable of the inner-loop state space. To impose the $f(0) = 0$ assumption, these terms can be manipulated by multiplying and dividing these terms by a state that will never go to zero. Because p, q, r and δp, δq, δr can all go to zero, an additional state s with stable dynamics is added to the state space in order to absorb the biases:

$$\dot{s} = -\lambda_s s \tag{54}$$

At each pass through the inner loop, s is set to its initial value (assumed small).

In the inner loop, a hard bound of 30 deg is imposed on the fin commands. This is achieved by replacing δp, δq, and δr in Eqs. (26–28) with saturation sine functions. That is,

$$\begin{bmatrix} \delta p \\ \delta q \\ \delta r \end{bmatrix} = \begin{bmatrix} sat\sin(30, \widetilde{\delta p}) \\ sat\sin(30, \widetilde{\delta q}) \\ sat\sin(30, \widetilde{\delta r}) \end{bmatrix} \tag{55}$$

where the actuator dynamics for $\widetilde{\delta p}$, $\widetilde{\delta q}$, and $\widetilde{\delta r}$ are modeled as first-order linear systems:

$$\dot{\widetilde{\delta p}} = -\lambda_p(\widetilde{\delta p} - u_p) \tag{56}$$

$$\dot{\widetilde{\delta q}} = -\lambda_q(\widetilde{\delta q} - u_q) \tag{57}$$

$$\dot{\widetilde{\delta r}} = -\lambda_r(\widetilde{\delta r} - u_r) \tag{58}$$

and the saturation sine function is defined as

$$sat\sin(m, z) = \begin{cases} m^*\sin(z) & \text{for} \quad |z| < \pi/2 \\ m & \text{for} \quad z \geq \pi/2 \\ -m & \text{for} \quad z \leq -\pi/2 \end{cases} \tag{59}$$

Thus, for the inner loop the state space is given by

$$\tilde{\boldsymbol{x}} = [p \quad q \quad r \quad s \quad \widetilde{\delta p} \quad \widetilde{\delta q} \quad \widetilde{\delta r}]^T \qquad \boldsymbol{u} = [u_p \quad u_q \quad u_r]^T \tag{60}$$

The inner-loop controller becomes

$$\boldsymbol{u} = -\tilde{R}_{\mathrm{IL}}(\tilde{\boldsymbol{x}})^{-1}\tilde{B}_{\mathrm{IL}}(\tilde{\boldsymbol{x}})^T\sum_{n=0}^{\infty}T_n^{\mathrm{IL}}(\tilde{\boldsymbol{x}}, \theta)\theta^n\begin{bmatrix} \boldsymbol{x}_T - \tilde{\boldsymbol{r}}_c \\ \boldsymbol{x}_N \end{bmatrix} \tag{61}$$

where

$$\tilde{\boldsymbol{r}}_c = [p_c \quad q_c \quad r_c]^T$$

$$\boldsymbol{x}_T = [p \quad q \quad r]^T, \qquad \boldsymbol{x}_N = [s \quad \widetilde{\delta p} \quad \widetilde{\delta q} \quad \widetilde{\delta r}]^T \tag{62}$$

We follow the same factorization form as Eq. (35). The corresponding inner-loop state-dependent coefficient factorization is given by[22]

$$\tilde{A}_{\mathrm{IL}}(\tilde{\boldsymbol{x}}) = \begin{bmatrix} a_{11} & a_{12} & a_{13} & a_{14} & a_{15} & a_{16} & a_{17} \\ a_{21} & a_{22} & a_{23} & a_{24} & a_{25} & a_{26} & a_{27} \\ a_{31} & a_{32} & a_{33} & a_{34} & a_{35} & a_{36} & a_{37} \\ 0 & 0 & 0 & -\lambda_s & 0 & 0 & 0 \\ 0 & 0 & 0 & 0 & -\lambda_p & 0 & 0 \\ 0 & 0 & 0 & 0 & 0 & -\lambda_q & 0 \\ 0 & 0 & 0 & 0 & 0 & 0 & -\lambda_r \end{bmatrix} \tag{63}$$

where

$$a_{11} = \frac{\bar{q}Sd^2}{2I_xV}C_{l_p}\cos\alpha, \qquad a_{12} = \frac{1}{2}\frac{I_y - I_z}{I_x}r$$

$$a_{13} = \frac{1}{2}\frac{I_y - I_z}{I_x}q - \frac{\bar{q}Sd^2}{2I_xV}C_{n_r}\sin\alpha$$

$$a_{14} = \frac{\bar{q}Sd}{sI_x}\left(C_{l_0}\cos\alpha - C_{n_0}\sin\alpha\right)$$

$$a_{15} = \frac{\bar{q}Sd}{I_x}\left(C_{l_{\delta p}}\cos\alpha - C_{n_{\delta p}}\sin\alpha\right)\frac{sat\sin(30, \widetilde{\delta p})}{\widetilde{\delta p}}$$

$$a_{16} = -\frac{\bar{q}Sd}{I_x}\left(C_{l_{\delta q}}\cos\alpha - C_{n_{\delta q}}\sin\alpha\right)\frac{sat\sin(30, \widetilde{\delta q})}{\widetilde{\delta q}}$$

$$a_{17} = -\frac{\bar{q}Sd}{I_x}\left(C_{l_{\delta r}}\cos\alpha - C_{n_{\delta r}}\sin\alpha\right)\frac{sat\,\sin(30,\widetilde{\delta r})}{\widetilde{\delta r}}$$

$$a_{21} = \frac{1}{2}\frac{I_z - I_x}{I_y}r, \qquad a_{22} = \frac{\bar{q}Sd^2}{2I_yV}C_{m_q}, \qquad a_{23} = \frac{1}{2}\frac{I_z - I_x}{I_y}p$$

$$a_{24} = \frac{\bar{q}Sd}{sI_y}C_{m_0}, \qquad a_{25} = \frac{\bar{q}Sd}{I_y}C_{m_{\delta p}}\frac{sat\,\sin(30,\widetilde{\delta p})}{\widetilde{\delta p}}$$

$$a_{26} = -\frac{\bar{q}Sd}{I_y}C_{m_{\delta q}}\frac{sat\,\sin(30,\widetilde{\delta q})}{\widetilde{\delta q}}$$

$$a_{27} = \frac{\bar{q}Sd}{I_y}C_{m_{\delta r}}\frac{sat\,\sin(30,\widetilde{\delta r})}{\widetilde{\delta r}}$$

$$a_{31} = \frac{1}{2}\frac{I_x - I_y}{I_z}q + \frac{\bar{q}Sd^2}{2I_zV}C_{l_p}\sin\alpha, \qquad a_{32} = \frac{1}{2}\frac{I_x - I_y}{I_z}p$$

$$a_{33} = \frac{\bar{q}Sd^2}{2I_zV}C_{n_r}\cos\alpha, \qquad a_{34} = \frac{\bar{q}Sd}{sI_z}\left(C_{l_0}\sin\alpha + C_{n_0}\cos\alpha\right)$$

$$a_{35} = \frac{\bar{q}Sd}{I_z}\left(C_{l_{\delta p}}\sin\alpha + C_{n_{\delta p}}\cos\alpha\right)\frac{sat\,\sin(30,\widetilde{\delta p})}{\widetilde{\delta p}}$$

$$a_{36} = -\frac{\bar{q}Sd}{I_z}\left(C_{l_{\delta q}}\sin\alpha + C_{n_{\delta q}}\cos\alpha\right)\frac{sat\,\sin(30,\widetilde{\delta q})}{\widetilde{\delta q}}$$

$$a_{37} = -\frac{\bar{q}Sd}{I_z}\left(C_{l_{\delta r}}\sin\alpha + C_{n_{\delta r}}\cos\alpha\right)\frac{sat\,\sin(30,\widetilde{\delta r})}{\widetilde{\delta r}}$$

The linear factorization is taken except that $\widetilde{sat}\,\widetilde{\sin}(30,\Delta)/\Delta$ replaces (Δ) wherever it appears. Δ represents $\widetilde{\delta p}$, $\widetilde{\delta q}$, or $\widetilde{\delta r}$.

Also

$$\tilde{B}_{\mathrm{IL}}(\tilde{\boldsymbol{x}}) = \begin{bmatrix} 0 & 0 & 0 \\ 0 & 0 & 0 \\ 0 & 0 & 0 \\ 0 & 0 & 0 \\ 1 & 0 & 0 \\ 0 & 1 & 0 \\ 0 & 0 & 1 \end{bmatrix} \tag{64}$$

V. Bank-to-Turn/Skid-to-Turn Command Logic

A hybrid BTT/STT autopilot command logic is used to convert the commanded accelerations from the guidance laws to reference-angle commands for the autopilot. In the midcourse and terminal phases of a missile flight, the BTT control is employed to prevent any engine flameout. As the missile approaches the end-game phase and passes a preset time-to-go threshold, BTT commands are executed simultaneously with STT commands to improve transient responses. During this interval, the missile is flying as a hybrid BTT/STT.

The BTT mode is broken into three commanded-acceleration magnitude regions in the inertial frame I as defined next[22]

If $a_c^I < 0.1g$, then STT control:

$$\mu_c = \mu \tag{65}$$

If $0.1g \le a_c^I < 1g$, then reduced BTT control:

$$\mu_c = \mu + \left[\tan^{-1}\left(-a_{y_c}^I \big/ a_{z_c}^I\right) - \mu\right]\left(a_c^I \big/ 1g\right) \tag{66}$$

If $a_c^I \ge 1g$, then full BTT control:

$$\mu_c = \tan^{-1}\left(-a_{\mathrm{yc}}^I \big/ a_{\mathrm{zc}}^I\right) \tag{67}$$

where $a_c^I = [a_{y_c}^I \;\; a_{z_c}^I]^T$ is the commanded acceleration in the inertial frame.

The idea of choosing command logic this way is to attempt to reduce the effect of noise affecting the controller. When the commanded acceleration is small, it is desired to make the error between commanded angles and actual angles small such that the controller would not respond to the noise if the noise magnitude is comparable to the commanded accelerations. As the commanded accelerations go up, the weight on errors would be increased accordingly. If above $1g$, the true desired angle commands are used.

In the full BTT mode,

$$\alpha_c = \left[(\|a_c\|m/\bar{q}S) - \left|\left(C_Z - C_{Z_\alpha}\alpha\right)\right|\right]\Big/\left|C_{Z_\alpha}\right|, \qquad \beta_c = 0 \tag{68}$$

where $a_c = [a_{y_c} \;\; a_{z_c}]^T$ is the commanded acceleration in the body frame.

In the reduced BTT mode,

$$\alpha_c = \left\{\left[(\|a_c\|m/\bar{q}S) - \left|\left(C_Z - C_{Z_\alpha}\alpha\right)\right|\right]\Big/\left|C_{Z_\alpha}\right|\right\}\cos(\mu_{\mathrm{full}} - \mu_c) \tag{69}$$

where absolute value is used to ensure that angle-of-attack command for BTT mode is positive.

$$\beta_c = \left\{\left[(\|a_c\|m/\bar{q}S) - \left|(C_Y - C_{Y_\beta}\beta)\right|\right]\Big/C_{Y_\beta}\right\}\sin(\mu_{\mathrm{full}} - \mu_c) \tag{70}$$

where

$$\mu_{\mathrm{full}} = \tan^{-1}\left(-a_{y_c}^I \big/ a_{z_c}^I\right) \tag{71}$$

Note that STT is used for small acceleration commands to prevent the missile from performing 180-deg rolls to achieve insignificant accelerations. STT control is also used in the end-game for quicker response.

In the STT mode,

$$\alpha_c = \left[\left(a_{z_c}m\big/\bar{q}S\right) - \left(C_Z - C_{Z_\alpha}\alpha\right)\right]\Big/C_{Z_\alpha}$$

$$\beta_c = \left[\left(a_{y_c}m\big/\bar{q}S\right) - \left(C_Y - C_{Y_\beta}\beta\right)\right]\Big/C_{Y_\beta}, \qquad \mu_c = \mu \tag{72}$$

As the missile approaches the end-game phase and passes a preset time-to-go threshold, the STT commands are switched into the BTT commands over a preselected time interval to attenuate transient responses,

$$\begin{bmatrix}\alpha_c \\ \beta_c \\ \mu_c\end{bmatrix} = \rho\begin{bmatrix}\alpha_c \\ \beta_c \\ \mu_c\end{bmatrix}_{\mathrm{STT}} + (1-\rho)\begin{bmatrix}\alpha_c \\ \beta_c \\ \mu_c\end{bmatrix}_{\mathrm{BTT}} \tag{73}$$

where ρ is a parameter that varies linearly from zero to one over the specified time interval.

VI. Simulation and Analysis of the Results

A. Simulation Setup

Numerical results are obtained using a six-degree-of-freedom BTT/STT missile model with a Simulink setup developed in Ref. 22. To ensure that the autopilot only command deflections are achievable, a 200 deg/s hard limit is imposed upon commanded roll rate p, pitch rate q_c, and yaw rate r_c, respectively. The limit of the commanded angle of attack α_c is set to 25 deg. The fin deflection limit is set to 30 deg. The actuator dynamics is modeled as a first-order system with a time constant of 0.01.

The goal of this study is to design an autopilot that maintains a good response throughout a wide flight envelope. The state weights on α_I, α, β_I, and β are varied at low, medium, and high altitudes until comparable performance is obtained over a range of altitudes. The state weights are chosen according to Ref. 22. They are curve fit to a quadratic function of dynamic pressure $\bar{q}$, which in turn is a function of missile velocity, one of the states in the outer loop.

$$\tilde{Q}(\tilde{\boldsymbol{x}})_{\mathrm{OL}} = \mathrm{diag}\{0, q_{22}(\tilde{\boldsymbol{x}}), q_{33}(\tilde{\boldsymbol{x}}), q_{44}(\tilde{\boldsymbol{x}}), q_{55}(\tilde{\boldsymbol{x}}), q_{66}(\tilde{\boldsymbol{x}}), 120\}$$

$$\tilde{R}(\tilde{\boldsymbol{x}})_{\mathrm{OL}} = \mathrm{diag}\{0.5, 1, 0.5\} \tag{74}$$

where diag{∗} represents the diagonal matrix;

$$q_{22}(\tilde{\boldsymbol{x}}) = 11.6742 \times 10^{-11}\bar{q}(\tilde{\boldsymbol{x}})^2 + 2.0182 \times 10^{-5}\bar{q}(\tilde{\boldsymbol{x}}) + 0.6137$$

$$q_{33}(\tilde{\boldsymbol{x}}) = 11.4251 \times 10^{-10}\bar{q}(\tilde{\boldsymbol{x}})^2 - 2.1170 \times 10^{-4}\bar{q}(\tilde{\boldsymbol{x}}) + 105.7985$$

$$q_{44}(\tilde{\boldsymbol{x}}) = q_{22}(\tilde{\boldsymbol{x}}), \qquad q_{55}(\tilde{\boldsymbol{x}}) = q_{33}(\tilde{\boldsymbol{x}})$$

$$q_{66}(\tilde{\boldsymbol{x}}) = 1.2 * \min\left\{100, [(\mu - \mu_c)180/\pi]^2 + 0.001\right\}$$

The inner-loop state and control weightings are chosen in a similar manner to those in the outer-loop design:

$$\tilde{Q}(\tilde{\boldsymbol{x}})_{\text{IL}} = \text{diag}\{16, q_{22}, q_{33}, 0, 0, 0, 0\}$$

$$\tilde{R}(\tilde{\boldsymbol{x}})_{\text{IL}} = \text{diag}\{0.04, 0.3, 0.06\} \tag{75}$$

where

$$q_{22} = 1.4609 \times 10^{-10}\bar{q}(\tilde{\boldsymbol{x}})^2 - 1.6816 \times 10^{-4}\bar{q}(\tilde{\boldsymbol{x}}) + 48.7078$$

$$q_{33} = 1.3880 \times 10^{-10}\bar{q}(\tilde{\boldsymbol{x}})^2 - 1.6573 \times 10^{-4}\bar{q}(\tilde{\boldsymbol{x}}) + 99.5426$$

$\tilde{Q}_0$ and $\tilde{Q}_x(\tilde{\boldsymbol{x}})$ required in the $\theta - D$ method [Eq. (10)] are chosen in the same manner as in the Eq. (35), that is, $\tilde{Q}_0 = \tilde{Q}(\tilde{x}_0)$ and $\tilde{Q}_x(\tilde{\boldsymbol{x}}) = \tilde{Q}(\tilde{\boldsymbol{x}}) - \tilde{Q}(\tilde{x}_0)$.

The time constants used the Eqs. (54) and (56–58) are given by

$$\lambda_p = \lambda_q = \lambda_r = \lambda_s = 1 \tag{76}$$

To show the effectiveness of the $\theta - D$ autopilot design for a wide flight envelope, the simulation is evaluated at three different flight conditions. The first condition is the initial design condition: flight Mach number $M = 2.7$ and flight altitude $h = 20{,}000$ ft. The second and third conditions are at $M = 2.7$, $h = 100$ ft (low-altitude flight) and $M = 2.7$, $h = 40{,}000$ ft (high-altitude flight), respectively. At the start of simulation, a commanded inertial acceleration of $a_{y_c} = 10g$, $a_{z_c} = -10g$ is fed into the system. These values are rotated into the body frame to be used as inputs to the BTT/STT command logic. Because these commanded accelerations are larger than $1g$, the missile responded in the BTT mode.

B. D_i Design with the $\theta - D$ Controller

In this simulation, the first three terms, that is, T_0, T_1, and T_2, in the control equation (16) are used to compute the necessary control. The simulation results will show that they are sufficient to achieve satisfactory performance. The $\theta - D$ outer/inner controller was designed based on the first flight condition. It was found that the controller worked very well for the second and third conditions using the same design parameters. The D_i matrices for the outer-loop controller were chosen as

$$D_1 = 0.9e^{-10t}\left\{-T_0\tilde{A}_{\text{OL}}(\tilde{\boldsymbol{x}})/\theta - \tilde{A}^T_{\text{OL}}(\tilde{\boldsymbol{x}})T_0\Big/\theta + T_0 g_0 R^{-1}[g^T(\tilde{\boldsymbol{x}})/\theta]T_0 + T_0[g(\tilde{\boldsymbol{x}})/\theta]R^{-1}g_0^T T_0 - \tilde{Q}_x(\tilde{\boldsymbol{x}})_{\text{OL}}/\theta\right\} \tag{77}$$

$$\begin{aligned} D_2 = 0.9e^{-10t}\Big\{&-T_1\tilde{A}_{\text{OL}}(\tilde{\boldsymbol{x}})/\theta - \tilde{A}^T_{\text{OL}}(\tilde{\boldsymbol{x}})T_1\Big/\theta \\ &+ T_0 g_0 R^{-1}[g^T(\tilde{\boldsymbol{x}})/\theta]T_1 + T_0[g(\tilde{\boldsymbol{x}})/\theta]R^{-1}g_0^T T_1 \\ &+ T_0[g(\tilde{\boldsymbol{x}})/\theta]R^{-1}[g^T(\tilde{\boldsymbol{x}})/\theta]T_0 + T_1 g_0 R^{-1}[g^T(\tilde{\boldsymbol{x}})/\theta]T_0 \\ &+ T_1[g(\tilde{\boldsymbol{x}})/\theta]R^{-1}g_0^T T_0 + T_1 g_0 R^{-1}g_0^T T_1\Big\} \end{aligned} \tag{78}$$

Note that in the outer-loop design $\tilde{B}(\tilde{\boldsymbol{x}})$ is state dependent; therefore, there would be a $g(\tilde{\boldsymbol{x}})$ term in D_1 and D_2. Also recall in remark 2.3 that θ is an intermediate variable that does not affect the results.

The inner-loop controller is designed with

$$D_1 = \text{diag}\{0, 0, 0, 0, 0.7e^{-t}, 0, 0.99e^{-0.01t}\} \times \left[-T_0\tilde{A}_{\text{IL}}(\tilde{\boldsymbol{x}})/\theta - \tilde{A}^T_{\text{IL}}(\tilde{\boldsymbol{x}})T_0\Big/\theta - \tilde{Q}_x(\tilde{\boldsymbol{x}})_{\text{IL}}/\theta\right] \tag{79}$$

$$D_2 = \text{diag}\{0.9e^{-5t}, 0, 0.9e^{-t}, 0, 0.9e^{-t}, 0, 0.99e^{-0.01t}\} \times \left[-T_1\tilde{A}_{\text{IL}}(\tilde{\boldsymbol{x}})/\theta - \tilde{A}^T_{\text{IL}}(\tilde{\boldsymbol{x}})T_1\Big/\theta + T_1 g_0 R^{-1}g_0^T T_1\right] \tag{80}$$

Note that in the inner-loop design $\tilde{B}(\tilde{\boldsymbol{x}})$ is a constant matrix, and so there would be no $g(\tilde{\boldsymbol{x}})$ term in D_1 and D_2.

As seen in Sec. II, D_i matrices play an important role in the $\theta - D$ method design. k_i and l_i in the D_i equations (17–19) are the design parameters. As pointed out in remark 2.2, they can be used to adjust the system performance as well as ensure the stability of the closed-loop system. The selection of (k_i, l_i) is based on the following method.

This approach is based on the observation that the $\theta - D$ approach gives an approximate closed-form solution to the SDRE

$$F^T(\boldsymbol{x})P(\boldsymbol{x}) + P(\boldsymbol{x})F(\boldsymbol{x}) - P(\boldsymbol{x})B(\boldsymbol{x})R^{-1}B^T(\boldsymbol{x})P(\boldsymbol{x}) + Q = 0 \tag{81}$$

where $F(\boldsymbol{x}) = A_0 + A(\boldsymbol{x})$.

To see this, assume that

$$\frac{\partial V}{\partial \boldsymbol{x}} = P(\boldsymbol{x})\boldsymbol{x} \tag{82}$$

and $P(\boldsymbol{x})$ is symmetric. Substituting Eq. (82) into the HJB equation (3) and writing nonlinear $\boldsymbol{f}(\boldsymbol{x})$ in a linear-like structure $\boldsymbol{f}(\boldsymbol{x}) = F(\boldsymbol{x})\boldsymbol{x} = [A_0 + A(\boldsymbol{x})]\boldsymbol{x}$ leads to the state-dependent Riccati equation (81). This is in fact the idea of the recently emerging SDRE technique.[16] Compared with the SDRE approach, the $\theta - D$ method solves a perturbed HJB equation (10) and assumes that

$$\frac{\partial V}{\partial \boldsymbol{x}} = \sum_{i=0}^{\infty} T_i(\boldsymbol{x}, \theta)\theta^i \boldsymbol{x} \tag{83}$$

As can be seen, the $\theta - D$ method is similar to the SDRE approach in the sense that both bring the nonlinear equation into a linear-like structure $\boldsymbol{f}(\boldsymbol{x}) = F(\boldsymbol{x})\boldsymbol{x}$ and solve the optimal control problem. The former gives an approximate closed-form solution, whereas the latter solves the algebraic Riccati equation at each state. It can be predicted that the $\theta - D$ solution is close to the SDRE solution, that is,

$$P(\theta - D) \approx P(\text{SDRE})$$

where

$$P(\theta - D) = \sum_{i=0}^{\infty} T_i(\boldsymbol{x}, \theta)\theta^i$$

is obtained from solving Eqs. (12–15) offline and $P(\text{SDRE})$ is obtained by solving Eq. (81) online.

An efficient procedure for finding the (k_i, l_i) was determined as follows: The SDRE controller is used to generate a state trajectory and then the maximum singular value of $P(\text{SDRE})$, that is, $\sigma_{\max}[P(\text{SDRE})]$, is computed at each state point. Similarly, the (k_i, l_i) parameters determine $P(\theta - D)$ and its associated $\sigma_{\max}[P(\theta - D)]$. Curve fits are then applied to $\sigma_{\max}[P(\text{SDRE})]$ and $\sigma_{\max}[P(\theta - D)]$, and the (k_i, l_i) are selected to minimize the difference between these singular value histories in a least-squares sense. The (k_i, l_i) can all be determined in one least-squares run offline.

C. Numerical Results and Analysis

Figure 2 shows the performance of the outer-/inner-loop autopilot at the first flight condition. The three figures on the left column of

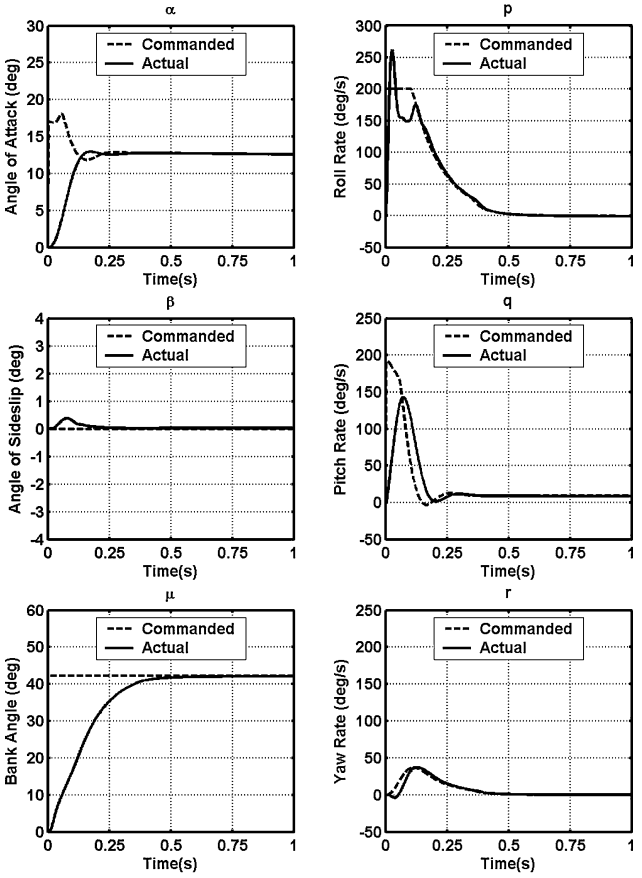

Fig. 2 Tracking responses of α, β, μ, p, q, and r, where $M = 2.7$ and $h = 20{,}000$ ft.

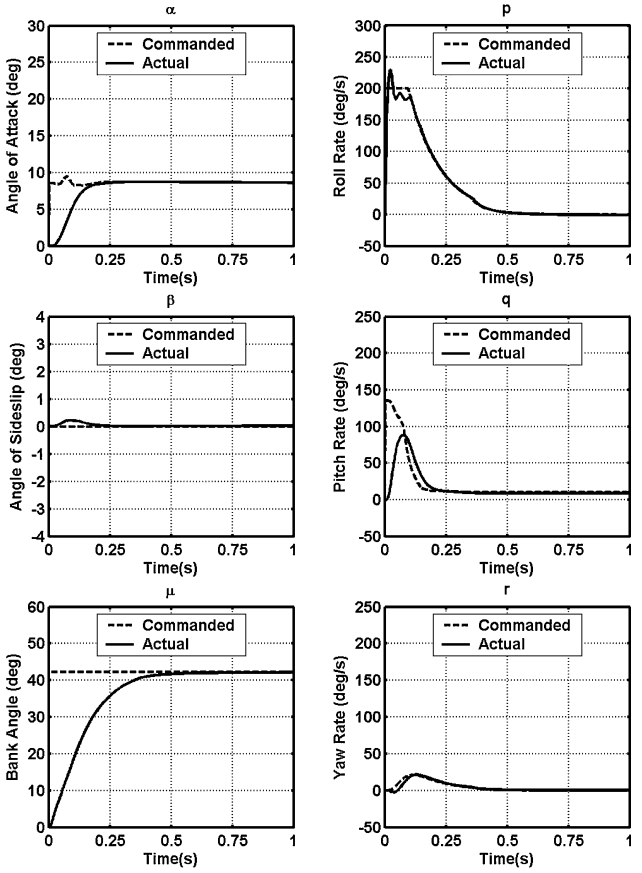

Fig. 3 Tracking responses of α, β, μ, p, q, and r, where $M = 2.7$ and $h = 100$ ft.

Fig. 2 demonstrate the outer-loop tracking, that is, α_c, β_c, and μ_c. The right column shows the inner-loop tracking, that is, p_c, q_c, and r_c. Likewise, the results for the second and third flight conditions are presented in Figs. 3 and 4, respectively. As can be seen, both the outer-loop and inner-loop controllers provide excellent tracking response over a large region of the operating envelope.

Figures 5–7 show the required fin deflections for these three cases. It can be seen that the fin deflections are all well behaved. Because the missile is flying in the BTT mode, the sideslip should be as small as possible. From the results of these three altitude simulations, it can be observed that the sideslip angle is kept at less than 1 deg throughout. It can also be seen that the settling time of the tracking responses at 40,000 ft is longer than the other two. This is because of the variation of the air density at high altitudes. Lower density at higher altitude leads to reducing aerodynamic forces and moments. The same commanded accelerations need bigger aerodynamic angles to achieve the necessary forces and moments. Therefore, the control response at 40,000 ft shows larger fin deflections compared to lower altitude cases. At 100-ft altitude, the missile goes through lowest angle of attack, sideslip angle, and control effort. Figure 8 presents the autopilot tracking of the acceleration commands coming from the guidance law. As can be seen, they are tracked very well in all three altitudes.

To evaluate the sensitivity of the autopilot design to speed, the autopilot designed at $M = 2.7$, $h = 20{,}000$ ft is also evaluated at two other different Mach numbers, $M = 2.0$ and 3.2. Figures 9–11 show the tracking responses and achieved fin deflections at these two Mach numbers, respectively.

It can be seen that the autopilot still performs very well. Note that at the higher Mach number the required angle of attack and control level are smaller than those at the lower Mach number. The reason is that aerodynamic coefficients associated with the aerodynamic angles and fin deflections are larger when the Mach number is higher. Also, at a given altitude the dynamic pressure is higher if the Mach

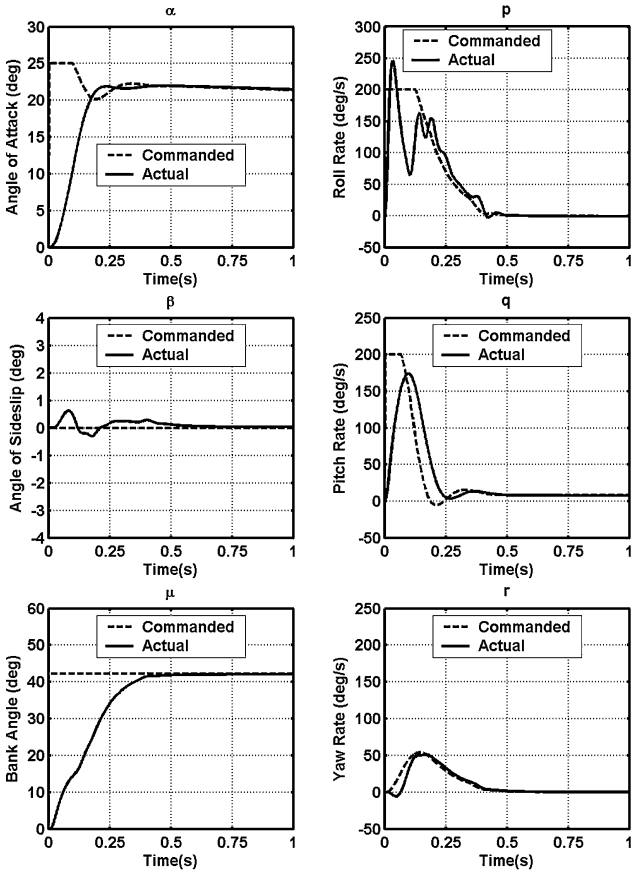

Fig. 4 Tracking responses of α, β, μ, p, q, and r, where $M = 2.7$ and $h = 40{,}000$ ft.

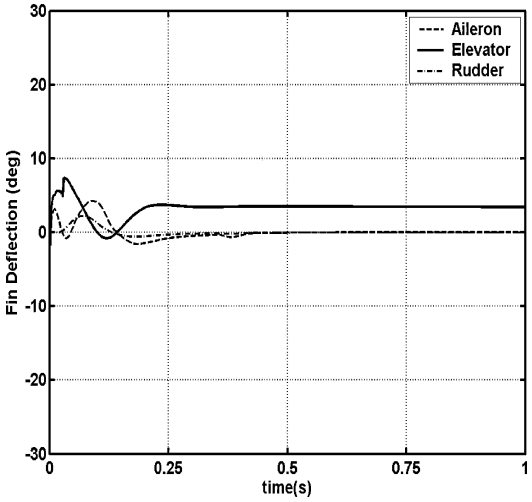

Fig. 5 Achieved fin deflections, where $M = 2.7$ and $h = 20{,}000$ ft.

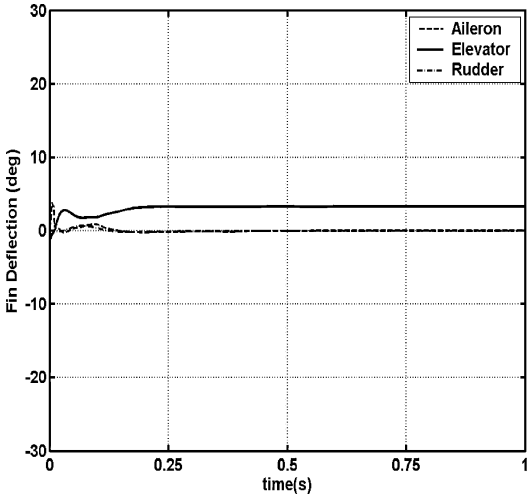

Fig. 6 Achieved fin deflections, where $M = 2.7$ and $h = 100$ ft.

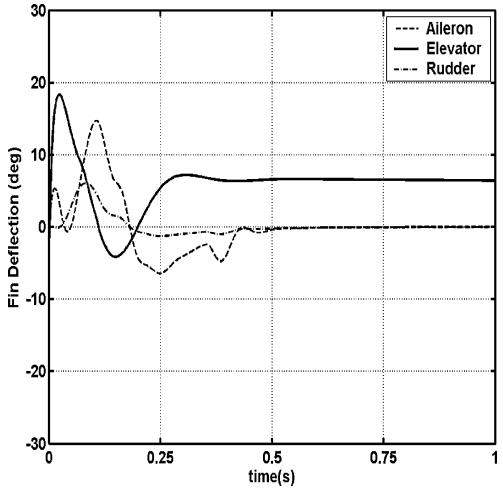

Fig. 7 Achieved fin deflections, where $M = 2.7$ and $h = 40{,}000$ ft.

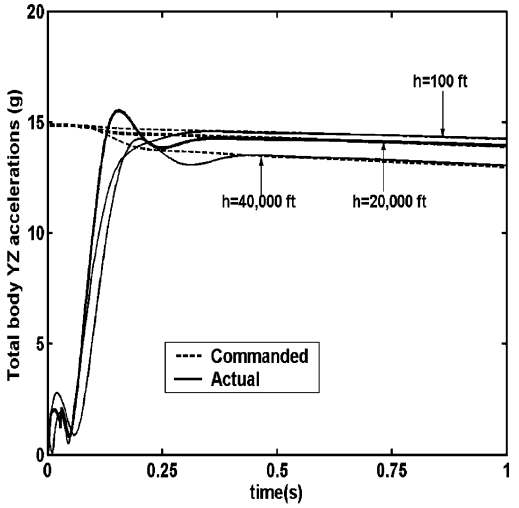

Fig. 8 Total body YZ acceleration tracking at different altitudes.

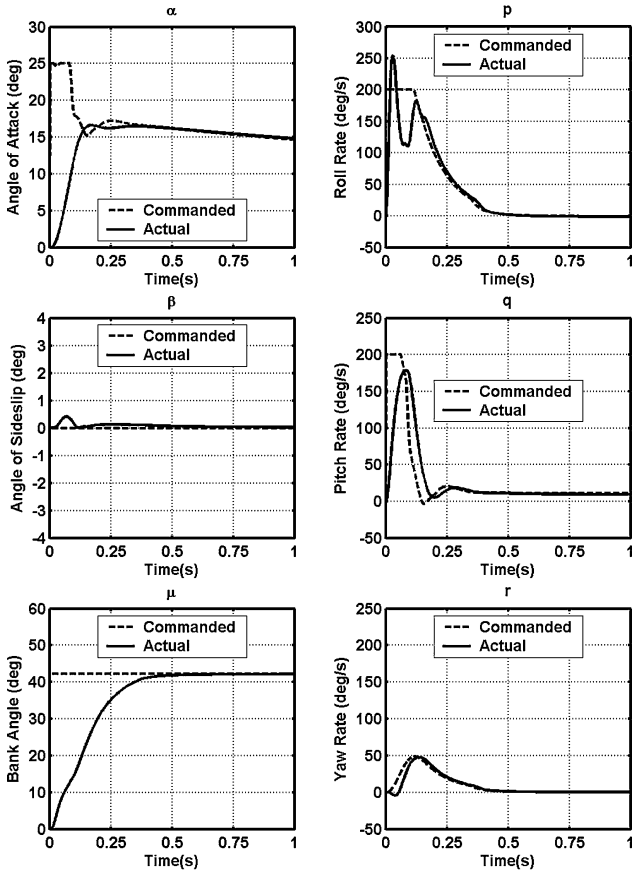

Fig. 9 Tracking response of α, β, μ, p, q, and r, where $M = 2.0$ and $h = 20{,}000$ ft.

number is higher. Thus for the same force commands, they need less aerodynamic angles α and β and fin deflections. Because the missile is flying at the BTT mode, the bank angle should be kept constant. Figure 12 demonstrates the comparison of bank-angle response at all the five different flight conditions. It can be seen that the autopilot performs very well in all these cases.

From the simulations, several advantages of the $\theta - D$ method can be observed. First, the $\theta - D$ outer-/inner-loop controllers show excellent tracking characteristics and are insensitive in operating flight conditions. Second, the $\theta - D$ based autopilot design is based on optimal control of a cost function. It allows the designer to consider the tracking performance and control energy in one integrated design. The third important advantage of the $\theta - D$ method is that it is available in closed-form expression if we take finite terms in Eq. (16). Compared with the SDRE technique,[22] the $\theta - D$ method does not need excessive online computations. This implementation advantage is more significant in the missile autopilot design problem because it involves 7×7 matrices in both outer- and inner-loop designs. Solving 7×7 Riccati equations online would be very time consuming. The final remark is that the tuning of design parameters

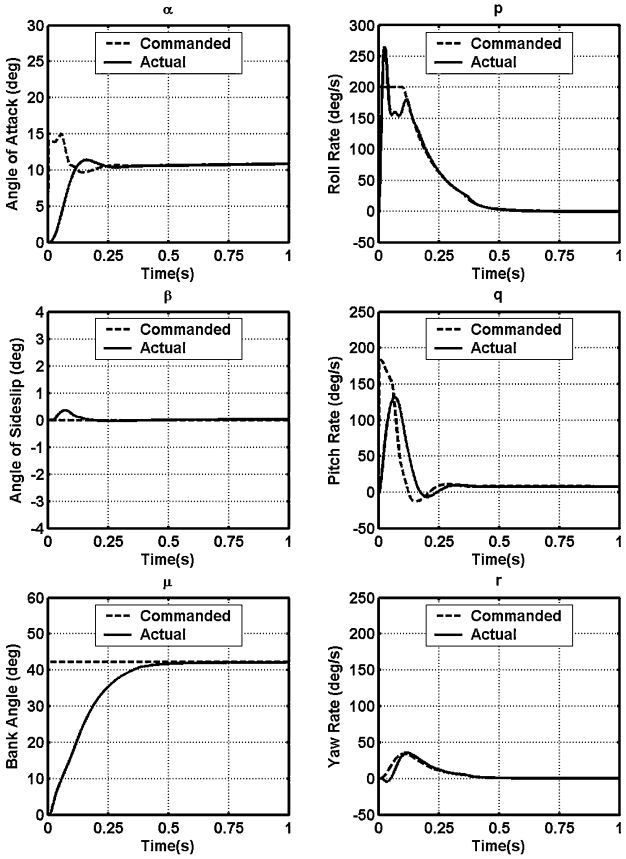

Fig. 10 Tracking response of α, β, μ, p, q, and r, where $M = 3.2$ and $h = 20{,}000$ ft.

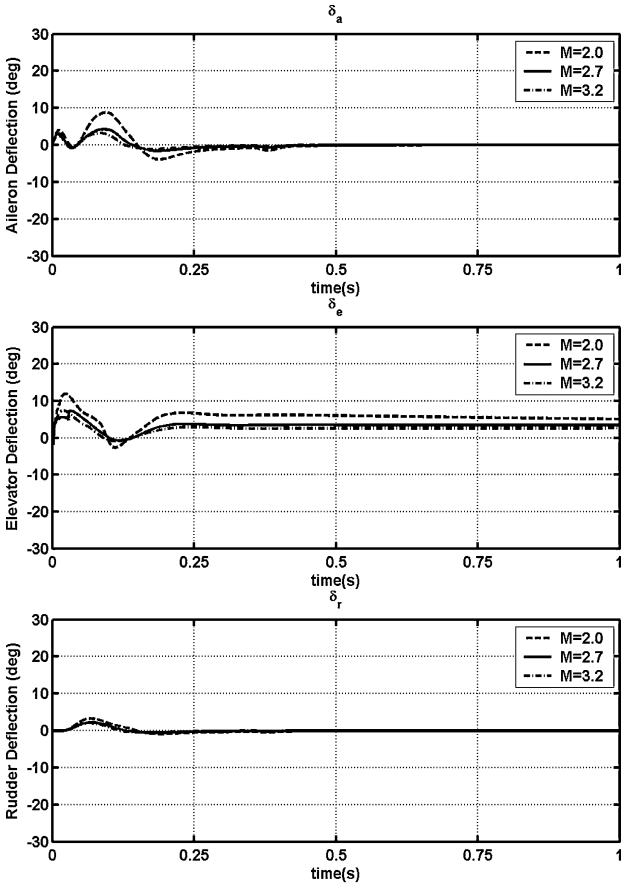

Fig. 11 Fin deflection comparison at different Mach numbers, where $h = 20{,}000$ ft.

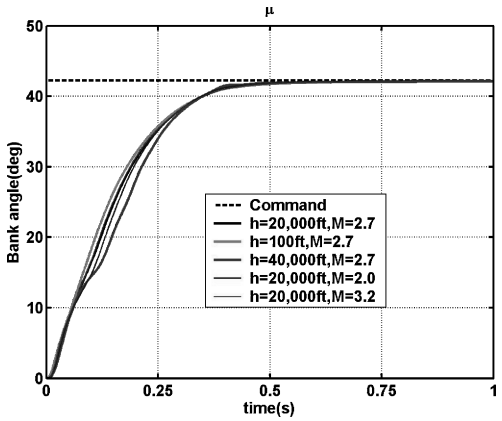

Fig. 12 Bank-angle comparison at different flight conditions.

in D_i matrices is not an involved process, which is shown in Section VI.B. Usually a diagonal matrix is picked and multiplied by the state-dependent terms, which are given in Eqs. (17–19). The numerical experiment also shows that system performance is not sensitive to the variations around the values of k_i and l_i in D_i.

VII. Conclusions

In this paper, a new nonlinear suboptimal control synthesis technique, $\theta - D$ method, has been used to design a hybrid bank-to-turn/skid-to-turn autopilot for a generic air-to-air missile. We formulate this autopilot design as an optimal control problem. Outer-loop and inner-loop control structures are used. The outer loop converts commanded angle of attack, sideslip, and bank angle to body-rate commands for the inner loop. The inner loop converts the body-rate commands to fin-deflection commands. The simulation results demonstrate excellent tracking performance and insensitivity to flight conditions over a wide flight envelope. The $\theta - D$ design gives a closed-form solution to this nonlinear optimal control problem and is easy to implement.

Acknowledgment

A grant from Anteon Corporation in support of this study for Naval Surface Warfare Center is gratefully acknowledged.

References

[1]Cloutier, J. R., Ever, J. H., and Feeley, J. J., "An Assessment of Air-to-Air Missile Guidance and Control Technology," *Proceedings of the American Control Conference*, IEEE Press, Piscataway, NJ, 1988, pp. 133–142.

[2]Williams, D. E., Friedland, B., and Madiwale, A. N., "Modern Control Theory for Design of Autopilots for Bank-to-Turn Missiles," *Journal of Guidance, Control, and Dynamics*, Vol. 10, No. 4, 1987, pp. 378–386.

[3]Krause, J., and Stein, G., "A General Adaptive Control Structure with a Missile Application," *Proceedings of the American Control Conference*, IEEE Press, Piscataway, NJ, 1988, pp. 561–566.

[4]Kamen, E. W., Bullock, T. E., and Song, C., "Adaptive Control Applied to Missile Autopilots," *Proceedings of the American Control Conference*, IEEE Press, Piscataway, NJ, 1988, pp. 555–560.

[5]Tan, W., Packard, A. K., and Balas, G. J., "Quasi-LPV Modeling and LPV Control of a Generic Missile," *Proceedings of the American Control Conference*, IEEE Press, Piscataway, NJ, 2000, pp. 3692–3696.

[6]Adams, R. J., and Banda, S. S., "Robust Flight Control Design Using Dynamic Inversion and Structured Singular Value Synthesis," *IEEE Transactions on Control Systems Technology*, Vol. 1, No. 2, 1993, pp. 80–92.

[7]Adams, R. J., Buffington, J. M., Sparks, A. G., and Banda, S. S., *Robust Multivariable Flight Control*, Springer-Verlag, London, 1994.

[8]McFarland, M. B., and D'Souza, C. N., "Missile Flight Control with Dynamic Inversion and Structured Singular Value Synthesis," *Proceedings of the AIAA Guidance, Navigation, and Control Conference*, AIAA, Washington, DC, 1994, pp. 544–550.

[9]Georgie, J., and Valasek, J., "Selection of Longitudinal Desired Dynamics for Dynamic Inversion Controlled Re-Entry Vehicles," AIAA Paper 2001-4382, Aug. 2001.

[10]Schumacher, C., and Khargonekar, P., "A Comparison of Missile Autopilot Designs Using H-Infinity Control with Gain Scheduling and Nonlinear Dynamic Inversion," *Proceedings of the American Control Conference*, IEEE Press, Piscataway, NJ, 1997, pp. 2759–2763.

[11]Wise, K. A., and Sedwick, J. L., "Nonlinear H_∞ Optimal Control for Agile Missiles," *Proceedings of the AIAA Guidance, Navigation, and Control Conference*, AIAA, Washington, DC, 1995, pp. 1295–1307.

[12]Thukral, A., and Innocenti, M., "A Sliding Mode Missile Pitch Autopilot Synthesis for High Angle of Attack Maneuvering," *IEEE Transactions on Control Systems Technology*, Vol. 6, No. 3, 1998, pp. 359–371.

[13]Salamci, M. U., and Ozgoren, M. K., "Sliding Mode Control with Optimal Sliding Surfaces for Missile Autopilot Design," *Journal of Guidance, Control, and Dynamics*, Vol. 23, No. 4, 2000, pp. 719–727.

[14]Bhat, M. S., and Powly, A. A., "Variable Structure Controller Design with Application to Missile Tracking," *Journal of Guidance, Control, and Dynamics*, Vol. 24, No. 4, 2001, pp. 859–862.

[15]Shkolnikov, I. A., and Shtessel, Y. B., "Robust Missile Autopilot Design Via High-Order Sliding Mode Control," AIAA Paper 2000-3968, Aug. 2000.

[16]Cloutier, J. R., D'Souza, C. N., and Mracek, C. P., "Nonlinear Regulation and Nonlinear H_∞ Control Via the State-Dependent Riccati Equation Technique," *Proceedings of the 1st International Conference on Nonlinear Problems in Aviation and Aerospace*, AIAA, Reston, VA, 1996, pp. 117–123.

[17]Xin, Ming, and Balakrishnan, S. N., "Robust State Dependent Riccati Equation Based Guidance Laws," *Proceedings of the American Control Conference*, IEEE Press, Piscataway, NJ, 2001, pp. 3352–3357.

[18]Menon, P. K., and Ohlmeyer, E. J., "Integrated Design of Agile Missile Guidance and Control Systems," *Proceedings of the 7th Mediterranean Conference on Control and Automation*, IEEE Control System Society, Piscataway, NJ, 1999, pp. 1469–1494.

[19]Wise, K. A., and Sedwick, J. L., "Nonlinear Control of Agile Missiles Using State Dependent Riccati Equations," *Proceedings of the American Control Conference*, IEEE Press, Piscataway, NJ, 1997, pp. 379, 380.

[20]Xin, Ming, and Balakrishnan, S. N., "A New Method for Suboptimal Control of a Class of Nonlinear Systems," *Proceedings of IEEE Conference on Decision and Control*, IEEE Press, Piscataway, NJ, 2002, pp. 2756–2761.

[21]Tournes, C., and Johnson, C. D., "Application of Linear Subspace Stabilization and Linear Adaptive Techniques to Aircraft Flight Control Problems," *Proceedings of the Thirtieth Southeastern Symposium on System Theory*, IEEE Press, Piscataway, NJ, 1998, pp. 146–150 (Part I), 151–155 (Part II).

[22]Cloutier, J. R., and Stansbery, D. T., "Nonlinear Hybrid Bank-to-Turn/Skid-to-Turn Missile Autopilot Design," AIAA Paper 2001-4158, Aug. 2001.

[23]Bryson, A. E., Jr., and Ho, Y. C., *Applied Optimal Control*, Hemisphere, New York, 1975.

[24]Cloutier, J. R., and Stansbery, D. T., "The Capabilities and Art of State-Dependent Riccati Equation-Based Design," *Proceedings of the American Control Conference*, IEEE Press, Piscataway, NJ, 2002, pp. 3352–3357.